Supporting Information

Silica-decorated Ni–Zn alloy as a highly active and selective catalyst for acetylene semihydrogenation

Wiyanti F. Simanullang,[a,†] Jiamin Ma,[a,†] Ken-ichi Shimizu,[a,b]

Shinya Furukawa,*[,a,b,c]

[a] *Institute for Catalysis, Hokkaido University, N-21, W-10, Sapporo 001-0021, Japan*

[b] *Elements Strategy Initiative for Catalysts and Batteries, Kyoto University, Katsura, Kyoto 615-8520, Japan*

[c] *Japan Science and Technology Agency, PRESTO, Chiyoda-ku, Tokyo 102-0076, Japan*

E-mail: furukawa@cat.hokudai.ac.jp,

Tel: +81-11-706-9162, Fax: +81-11-706-9163

[†] These authors equally contributed.

Experimental details

Catalyst Preparation

Ni and Ni–Zn alloy nanoparticles supported on silica (Ni/SiO_2 and $Ni–Zn/SiO_2$, Ni loading: 2 wt%) were prepared by pore-filling impregnation method. Aqueous solution of Ni $(NO_3)_3 \cdot 6H_2O$ (Wako, 99%) alone or Ni $(NO_3)_3 \cdot 6H_2O$ and Zn $(NO_3)_2 \cdot 6H_2O$ (Wako, 99%) with molar ratio 1:1 were added to dried silica gel (CARiACT G-6, Fuji Silysia, S_{BET} = 470 m^2g^{-1}) so that the solutions filled the silica pores. The mixtures were sealed overnight at room temperature and dried over liquid nitrogen under vacuum overnight followed by drying at 90℃. The reduction under flowing H_2 at 600 ℃ for 1 h was then performed. Silica decorated Ni ($Si–Ni/SiO_2$) and Ni–Zn nanoparticles supported on silica ($Si–Ni–Zn/SiO_2$) were prepared by adding ethanol solution of $C_{18}H_{16}OSi$ (Mr = 276.40 g mol^{-1}, Tokyo Chemical Industry Co., Ltd) and Ni $(NO_3)_3 \cdot 6H_2O$ (Wako, 99%) with Zn $(NO_3)_2 \cdot 6H_2O$ (Wako, 99%) in a similar fashion to that of Ni/SiO_2 or $Ni–Zn/SiO_2$ except drying over the hot plate. The specific surface area of the prepared catalysts were as follows: $Ni–Zn/SiO_2$, S_{BET} = 454 m^2g^{-1}; $Si–Ni–Zn/SiO_2$, S_{BET} = 451 m^2g^{-1}, indicating that the silica-decoration did not decrease the surface area.

Reaction condition

The catalytic activities of the prepared catalysts were tested in hydrogenation of acetylene. The mixture of Ni-based catalysts (15 mg) and quartz sand (Miyazaki Chemical Co., 250 ~ 420 μm, 2 g) was filled into a quartz glass tube (internal diameter, 10 mm) and put in a fixed bed continuous reactor. Prior to the activity test, the catalyst was reduced under flowing H_2 (10 mL min^{-1}) at 500℃ for 0.5 h and the temperature was cooled down to the reaction temperature. The reaction was initiated by flowing the gas mixture: (C_2H_2:H_2:He = 2:20:10 mL min^{-1}: GHSV = 128,000 mL h^{-1} g^{-1}). The gas phase was analyzed by an online thermal conductivity detector (TCD) gas chromatography (Shimadzu GC-8A) equipped downstream connected to the Unipack S packed column. The catalytic performance (C_2H_2 conversion and C_2H_4 selectivity) at 15 min on stream was reported. For the stability test, 60 mg of catalyst was used. C_2H_2 conversion and C_2H_4 selectivity were calculated using the following equations:

$$C_2H_2 \text{ conversion (\%)} = (F_{C2H2,in} - F_{C2H2,out}) / F_{C2H2,in} \times 100$$

$$C_2H_4 \text{ selectivity (\%)} = F_{C2H4,out} / (F_{C2H2,in} - F_{C2H2,out}) \times 100$$

Characterization

The crystal structure of the prepared catalyst was examined by powder X-ray diffraction (XRD) using

a Rigaku MiniFlex II/AP diffractometer with Cu Kα radiation.

High-angle annular dark field scanning transmission electron microscopy (HAADF-STEM) was carried out using a JEOL JEM-ARM200 M microscope equipped with an energy dispersive X-ray (EDX) analyzer (EX24221M1G5T). STEM analysis was performed at an accelerating voltage of 200 kV. To prepare the TEM specimen, all samples were sonicated in ethanol and then dispersed on a Mo grid supported by an ultrathin carbon film.

Reduction properties of the as-prepared catalyst were analyzed by temperature programmed reduction method by H_2 (H_2-TPR) by using a BELCAT-Ⅱ instrument. Prior to analysis, 30 mg of catalyst was pretreated at 150°C for 1 h under inert He flow to remove absorbed water, then the sample was heated under H_2 flow (5v% H_2 balanced with Ar 30 sccm) in the temperature from 50°C to 900°C at a ramping rate of 2°C/min^{-1}.

Computational Details

Periodic density functional theory (DFT) calculations, except frequency calculations, were performed using the CASTEP code[1] with Vanderbilt-type ultrasoft pseudopotentials[2] and a revised Perdew–Burke–Ernzerhof exchange-correlation functional (RPBE)[3] based on the generalized gradient approximation (GGA). The plane-wave basis set was truncated at a kinetic energy of 370 eV. A Fermi smearing of 0.1 eV was utilized. The reciprocal space was sampled using a *k*-point mesh with a typical spacing of 0.04 $Å^{-1}$ generated by the Monkhorst–Pack scheme.[4] Geometry optimizations were performed in supercell structures using periodic boundary conditions. Surfaces were modeled using 4 atomic layer-thick metallic slabs. An $L1_2$-type Ni_3Zn structure was considered as the model of the $Ni_{0.75}Zn_{0.25}$ alloy. The surface was modeled using $Ni_3Zn(111)$ and $Ni_3Zn(211)$ planes for the terrace and step sites of Ni–Zn, respectively, with a 13 Å vacuum region. Convergence criteria comprised a) a self-consistent field (SCF) tolerance of 1.0×10^{-6} eV/atom, b) an energy tolerance of 1.0×10^{-5} eV/atom, c) a maximum force tolerance of 0.05 eV $Å^{-1}$, and d) a maximum displacement tolerance of 1.0×10^{-3} Å for structure optimization and energy calculation. Frequency calculations of adsorbed CO

molecules were conducted by the DMol[3] code[5] based on the aforementioned optimized structures. These calculations involved the RPBE functional, a double-numeric quality basis set with polarization functions (DNP, comparable to Gaussian 6-311G**)[6] with a real-space cutoff of 4.2 Å, DFT semi-core pseudopotential core treatment,[7] and a Fermi smearing of 0.1 eV. The SCF convergence was accelerated using the iterative scheme proposed by Kresse and Furthmüller.[8] The partial Hessian matrix including C and O atoms was computed to evaluate the harmonic frequencies for adsorbed CO. All computed harmonic frequencies were scaled by an empirical factor of 1.056, which corresponds to the ratio of experimental[9] and computed values for gas-phase CO (2143 cm^{-1}/2028.7 cm^{-1}).

Supplementary Figures

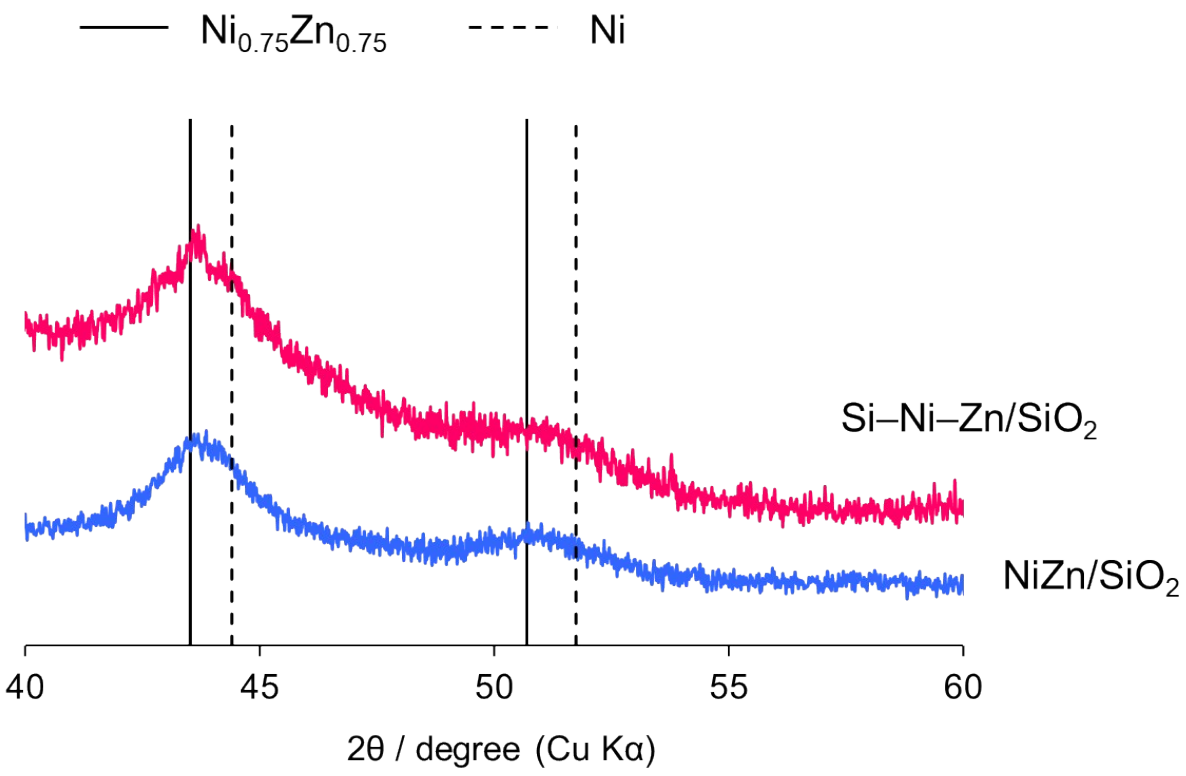

Fig. S1. XRD patterns of Ni–Zn/SiO_2 and Si–Ni–Zn/SiO_2. References are shown as black vertical lines.

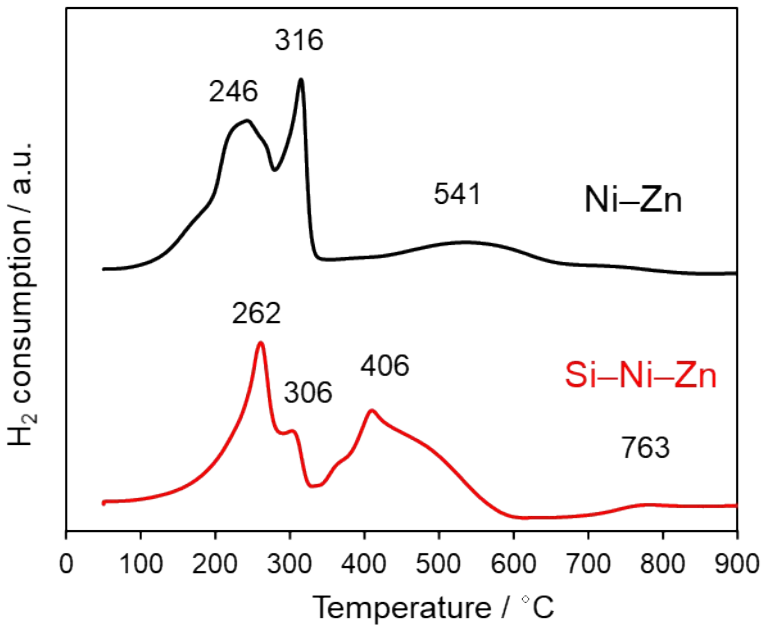

Fig. S2. H_2-TPR profiles of Ni–Zn/SiO_2 and Si–Ni–Zn/SiO_2.

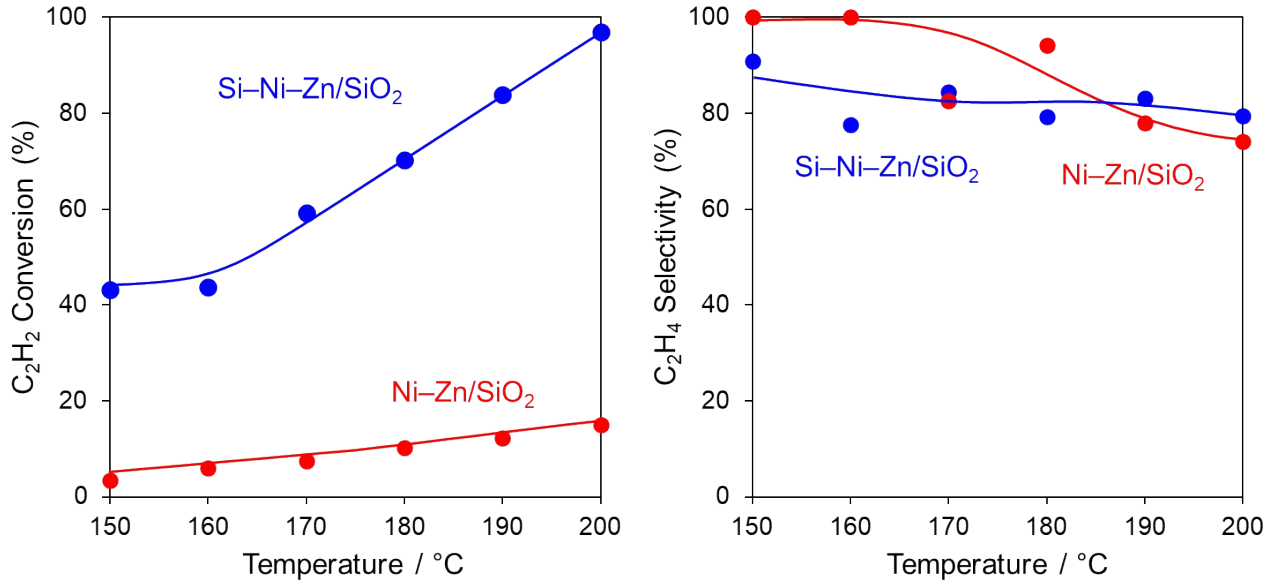

Fig. S3. Temperature-dependences of C_2H_2 conversion and C_2H_4 selectivity for Ni–Zn/SiO_2 and Si–Ni–Zn/SiO_2 catalysts.

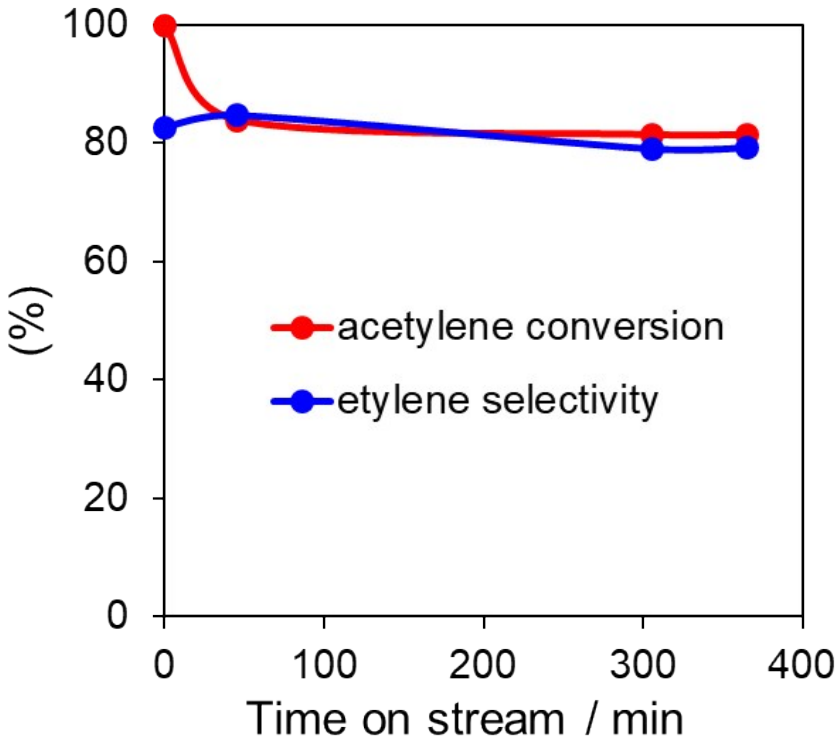

Fig. S4. Stability test for acetylene semihydrogenation using Si–Ni–Zn/SiO_2.

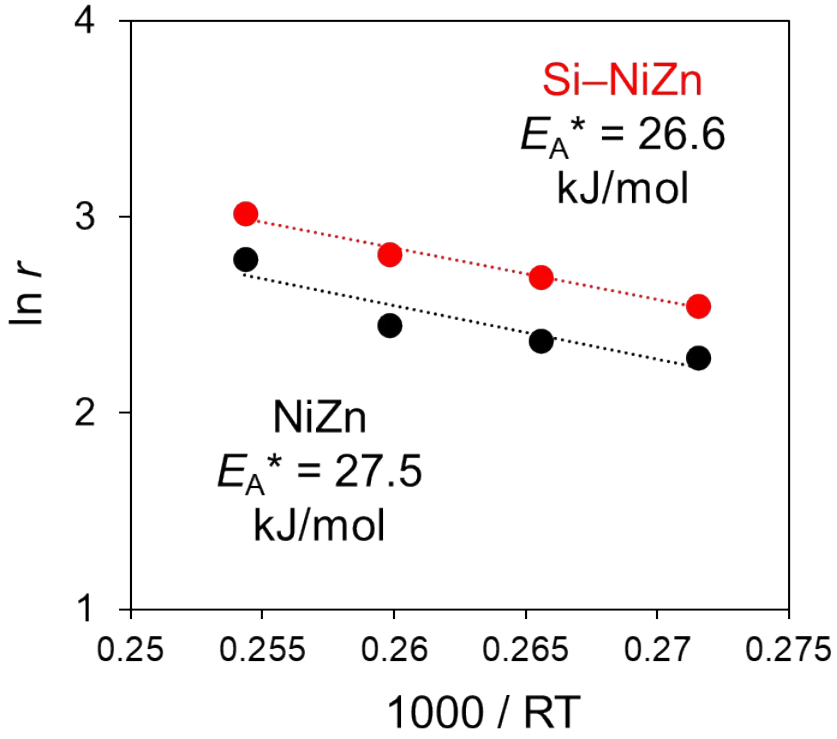

Fig. S5. Arrhenius-type plots obtained in acetylene semihydrogenation on Ni–Zn/SiO_2 and Si–Ni–Zn/SiO_2.

Table S1. Summary of the catalytic performance of Ni-based catalyst in acetylene semihyderogenation.

entry	catalyst	Ni wt%	amount / mg	C_2H_2 flow /mLmin^{-1}	C_2H_2:H_2:C_2H_4:He(Ar) / mLmin^{-1}	GHSV / mLg^{-1}h^{-1}	conv. (%)	sel. (%)	temp. / °C	specific rate / $mL_{C2H2}min^{-1}g_{Ni}^{-1}$	ref
1	Si–Ni–Zn/SiO_2	2	15	2	2:20:0:10	128,000	97	80	200	6,467	this work
2	$NiCu_{0.125}$/MCM-41	1	100	3.3	3.3:10:0:0	8,000	100	63	250	3,333	10
3	$AgNi_{0.125}/SiO_2$	0.37	30	0.3	0.3:6:6:17.7	60,000	98	25	200	2,649	11
4	Ni_3Ge/MCM-41	3.2	15.6	3.9	3.9:8.1:0:17	111,360	30	87	250	2340	12
5	Ni–Zn/SiO_2	2	15	2	2:20:0:10	128,000	15	80	200	1,007	this work
6	NiGa	10	50	1.2	1.2:12:24:82.5	144,000	90	82	190	216	13
7	$Ni_3Ga/MgAl_2O_4$	2	100	0.33	0.33:6.7:33.3:26.67	40,000	92	77	220	153	14
8	Ni/MCM-41	25	100	3.7	3.7:7.4:0:55.5	40,000	96	87	240	142	15
9	Ni–CeO_2	1.54	200	0.35	0.35:24.5:1.4:43.75	21,000	100	100	200	114	16
10	Ni_6In/SiO_2	8	500	3	3:30:0:267	36,000	100	64	200	75	17
11	Na-Ni/CHA	3.5	200	0.5	0.5:8:0:41.5	15,000	100	97	170	71	18
12	Ni-SAs/N-C	5.67 [a]	400	0.2	0.2:4:20:15.8	6,000	96	91	200	8	19

[a] Although the loading amount of Ni was not reported, it was estimated from the original Ni content[20] and the weight loss by TG.

Supplementary references

1. M. D. Segall, P. J. D. Lindan, M. J. Probert, C. J. Pickard, P. J. Hasnip, S. J. Clark, M. C. Payne, *J. Phys. Condens. Matter* 2002, **14**, 2717–2744.
2. D. Vanderbilt, *Phys. Rev. B* 1990, **41**, 7892–7895.
3. B. Hammer, L. B. Hansen, J. K. Norskov, *Phys. Rev. B* 1999, **59**, 7413–7421.
4. H. J. Monkhorst, J. D. Pack, *Phys. Rev. B* 1976, **13**, 5188–5192.
5. B. Delley, *J. Chem. Phys.* 1990, **92**, 508–517.
6. Y. Inada, H. Orita, *J. Comput. Chem.* 2008, **29**, 225–232.
7. B. Delley, *Phys. Rev. B* 2002, **66**, 155125.
8. G. Kresse, J. Furthmuller, *Phys. Rev. B* 1996, **54**, 11169–11186.
9. D. Scarano, S. Bordiga, C. Lamberti, G. Spoto, G. Ricchiardi, A. Zecchina, C. O. Arean, *Surf. Sci.* 1998, **411**, 272–285.
10. S. Zhou, L. Kang, X. Zhou, Z. Xu, M. Zhu, *Nanomaterials*, 2020, **10**, 509.
11. G. Xian, P. Xiao, Y. Liu, A. Wang, Y. Su, L. Li, T. Zhang, *Appl. Catal. A: Gen.*, 2017, **545**, 90–96.
12. T. Komatsu, K. Sou, K. Ozawa, *J. Mol. Catal. A: Chem.*, 2010, **319**, 71–77.
13. Y. Cao, H. Zhang, S. Ji, Z. Sui, Z. Jiang, D. Wang, Y. Li, *Angew. Chem. Int. Ed.*, 2020, **132**, 11744–11749.
14. Y. Liu, X. Liu, Q. Feng, D. He, L. Zhang, C. Lian, R. Shen, G. Zhao, Y. Ji, D. Wang, G. Zhou, Y. Li, *Adv. Mater.*, 2016, **28**, 4747–4754.
15. J. Zhao, L. He, J. Yu, Y. Shi, R. Miao, Q. Guan. P. Ning, *New J. Chem.*, 2021, **45**, 1054–1062.
16. C. Riley , A. D. La Riva , S. Zhou , Q. Wan , E. J. Peterson , K. Artyushkova , M. D. Farahani , H. B. Friedrich , L. K. Burkemper and N. Atudorei , *ChemCatChem*, 2019, **11** , 1526–1533.
17. Y. Chen, J. Chen, *Appl. Surf. Sci.*, 2016, **387**, 16-27.
18. Y. Chai, G. Wu, X. Liu, Y. Ren, W. Dai, C. Wang, Z. Xie, N. Guan, L. Li, *J. Am. Chem. Soc.* 2019, **141**, 9920–992.
19. X. Dai, Z. Chen, T. Yao, L. Zheng, Y. Lin, W. Liu, H. Ju, J. Zhu, X. Hong, S. Wei, Y. Wu and Y. Li, *Chem. Commun.*, 2017, **53**, 11568–11571.
20. R. Li, X. Ren, X. Feng, X. Li, C. Hu, B. Wang, *Chem. Commun.*, 2014, **50**, 6894-6897.